NASA-TM - 88255

NASA Technical Memorandum 88255

NASA-TM-88255 19860018588

Rotor/Wing Aerodynamic Interactions in Hover

Fort F. Felker and Jeffrey S. Light

May 1986

National Aeronautics and
Space Administration

NASA Technical Memorandum 88255

Rotor/Wing Aerodynamic Interactions in Hover

Fort F. Felker,
Jeffrey S. Light, Ames Research Center, Moffett Field, California

May 1986

NASA
National Aeronautics and
Space Administration

Ames Research Center
Moffett Field, California 94035

N86-28060 #

ROTOR/WING AERODYNAMIC INTERACTIONS IN HOVER

Fort F. Felker and Jeffrey S. Light
Aerospace Engineers
NASA Ames Research Center
Moffett Field, California

Abstract

An experimental and theoretical investigation of rotor/wing aerodynamic interactions in hover is described. The experimental investigation consisted of both a large-scale and a small-scale test. A 0.658-scale, V-22 rotor and wing was used in the large-scale test. Wing download, wing surface pressure, rotor performance, and rotor downwash data from the large-scale test are presented. A small-scale experiment was conducted to determine how changes in the rotor/wing geometry affected the aerodynamic interactions. These geometry variations included the distance between the rotor and wing, wing incidence angle, and configurations both with the rotor axis at the tip of the wing (tilt rotor configuration) and with the rotor axis at the center of the wing (compound helicopter configuration). A wing with boundary-layer control was also tested to evaluate the effect of leading and trailing edge upper surface blowing on the wing download. A computationally efficient, semi-empirical theory was developed to predict the download on the wing. Finally, correlations between the theoretical predictions and test data are presented.

Nomenclature

A = rotor disc area, πR^2, m^2

C_T = rotor thrust coefficient, $T/\rho A V_{tip}^2$

c = wing chord, m

DL = wing download, N

h = blowing slot height, m

P = pressure, N/m^2

P_{atm} = atmospheric pressure, N/m^2

P_p = blowing slot plenum pressure, N/m^2

ΔP = differential pressure, $P - P_{atm}$, N/m^2

R = rotor radius, m

R_c = maximum radius of chordwise flow on wing, m

T = rotor thrust, N

V = rotor downwash velocity, m/s

V_H = ideal induced velocity in hover, $\sqrt{T/2\rho A}$, m/s

V_{tip} = rotor tip speed, m/s

x = wing chordwise location, m

z = distance between rotor and wing, m

α = wing incidence angle, angle between wing chord line and horizontal, positive nose up, degree

δ_F = flap deflection angle, degree

ρ = air density, kg/m^3

Introduction

Rotor/wing aerodynamic interactions can have a dramatic effect on the hover performance of a tilt rotor aircraft or compound helicopter. For example, the download on the wing of a tilt rotor aircraft in hover can be as large as 15% of the total rotor thrust (Refs. 1 and 2). This adverse aerodynamic interference causes a significant reduction in the payload of the aircraft. Since the payload of a tilt rotor is typically 25-30% of the aircraft's gross weight, small changes in the wing download can have a large effect on the size of the payload. Some previous investigations on rotor/wing aerodynamic interactions are reported in Refs. 3-6.

This paper describes an experimental and theoretical investigation of rotor/wing aerodynamic interactions in hover. The experimental program consisted of large- and small-scale tests. A semi-empirical theory was developed using flow visualization and rotor downwash data acquired in the large-scale test.

A 0.658-scale, V-22 rotor and wing were used in the large-scale test. Wing forces and moments,

---

Presented at the 42nd Annual Forum of the American Helicopter Society, Washington, D.C., June 2-4, 1986.

wing surface pressures, rotor performance, and rotor downwash velocities were measured. Flow visualization was accomplished with tufts and smoke. The effect of changes in the rotor thrust on wing download was measured, as well as the effect of the wing on rotor performance. This test was sponsored by the U.S. Naval Air Systems Command, and support for the test was provided by Boeing Vertol under contract to the U.S. Navy.

The small-scale test was designed to evaluate the effect of changes in the rotor/wing geometry on the wing download in hover. These rotor/wing geometry variations included the distance between the rotor and wing, wing incidence angle, and configurations both with the rotor axis at the tip of the wing (tilt rotor configuration) and with the rotor axis at the center of the wing (compound helicopter configuration). Measurements were made of wing forces and moments, wing surface pressures, and rotor performance. The rotor was a 0.16-scale model of the Sikorsky S-76 rotor system. Two wings were tested: a conventional wing with a 25% plain flap, and a wing with boundary-layer control slots at the leading and trailing edges. Both wings had the same chord and span.

A semi-empirical theory that predicts the wing download was developed using data acquired in the large-scale test. The theory uses experimental data on rotor downwash velocities, wing surface flow directions, and wing section drag coefficients to compute the wing download. The theoretical predictions have been correlated with wing download data with good results.

This paper describes the first comprehensive investigation of rotor/wing aerodynamic interactions in hover, covering a wide range of realistic geometries. The fundamental aerodynamic phenomena associated with the rotor/wing flow field have been identified, as well as the dominant mechanisms of wing download. Finally, the first attempt to reduce wing download by using boundary-layer control is described.

Description of Test Apparatus

The tests were conducted at the Ames Outdoor Aerodynamic Research Facility, which consists of a 30-m square concrete pad, a below-ground-level frame for attaching model support struts, and an underground control room with a complete data acquisition system. The Facility is located sufficiently remote from other buildings that there is no aerodynamic interference (except with the ground). Testing was conducted in low winds, such that the ratio of wind speed to rotor downwash velocity was small.

Large Scale Test

A 0.658-scale model of a V-22 rotor and wing was used in the large-scale experiment (Fig. 1). The rotor axis was horizontal to reduce aerodynamic interactions between the rotor and the ground. The rotor had three blades with a radius of 3.81 m. The blades were dynamically and geometrically similar to V-22 rotor blades, except that the solidity was 8% greater than the current V-22 rotor configuration. Rotor system characteristics are summarized in Table 1. Rotor performance was measured by a six-component rotor balance system. Rotor downwash velocities with the wing removed were measured by a wake rake. Further information on this rotor system can be found in Ref. 7.

The wing was installed in the wake of the rotor at a position representative of a V-22 aircraft in hover. An image plane was installed to represent the plane of symmetry of the aircraft, and to simulate the presence of the second rotor and wing on an actual aircraft. The image plane was square, measuring 2.2 rotor radii on each side. It was located 1.21 rotor radii from the rotor axis, and the rotor hub was positioned above the center of the plane. The wing, rotor, and image plane installation is shown in Fig. 1. The wing geometry and the locations of the pressure taps are summarized in Table 2. The wing airfoil was developed at Bell Helicopter specifically for use on the V-22 wing, and is designated an A821201. The wing was mounted on its own six-component balance system, so that wing forces and moments could be independently measured. Six chordwise rows of pressure taps were installed on the upper and lower surfaces of the wing.

Small Scale Tests

A 0.16-scale model of the Sikorsky S-76 rotor was used in the small-scale test (Fig. 2). The blades were dynamically and geometrically similar to Sikorsky S-76 blades, except that the model blades had rectangular tips instead of swept-tapered tips. Rotor system characteristics are summarized in Table 3. The rotor plane was 2.86 rotor radii above the ground.

The rotor was installed on the Ames Rotor Test Rig (RTR). A six-component internal strain-gage balance was used to measure steady-state rotor forces and moments. Three single-axis load cells were installed between the RTR and its support stand to provide redundant measurements of the rotor thrust.

Two wings were used in this test, a conventional wing and a "circulation control" wing with boundary-layer control blowing slots. The conventional wing used was a NACA 23015 airfoil with a

25% chord plain flap. The flap angle could be varied from 0 to 90°. The circulation control wing airfoil is similar to that used for an X-wing aircraft (Fig. 3). The wing had blowing slots at both the leading and trailing edges. The airflow through the slots was varied either by changing the slot height or by changing the air pressure in the two wing plenums. These plenums, one for the leading edge and one for the trailing edge, allowed for testing of the effect of differential blowing on the wing download. The characteristics of the two wings are outlined in Table 4.

Mean wing surface pressure data were obtained for both wings. This was accomplished using pressure taps set in five chordwise rows and one spanwise row.

The rotor was operated with the rotor thrust down and the wake of the rotor traveled up into the wing. The wings were mounted upside down on a model support system and balance. This system allowed for unobstructed flow between the rotor and the wing. Throughout this paper, references to the "upper" and "lower" surfaces of the wing refer to the normal upper and lower wing surfaces of the wing, and not the test setup (Fig. 2). A sketch of the rotor and wing installation is provided in Fig. 4.

Many rotor/wing geometry variations were possible using the positioning mechanisms on the support system. These variations included the distance between the rotor and wing, wing incidence angle, and configurations both with the rotor axis at the tip of the wing (tilt rotor configuration) and with the rotor axis at the center of the wing (compound helicopter configuration). When testing with the rotor axis at the wing tip, an image plane was installed to simulate the presence of a second rotor and wing on a tilt rotor aircraft. This image plane was square, measuring 0.86 rotor radii on each side, and was installed 1.29 rotor radii from the rotor axis. Wing forces and moments were measured using a six-component internal strain-gage balance.

Effect of Wing and Image Plane on Large-Scale Rotor Performance

Four configurations were tested in the large-scale test. These were: isolated rotor; rotor, plus image plane; rotor, plus wing; and rotor, plus image plane, plus wing. The rotor figure of merit measured with these configurations is presented in Fig. 5. These data were acquired at full-scale tip speed and in low winds. The rotor performance data have been corrected for the effect of the wind. For the details of this correction procedure, and other test results, see Ref. 7.

The rotor performance with the wing installed was greater than the isolated rotor performance. For constant rotor power, the rotor thrust was increased by about 3% because of the aerodynamic interactions between the rotor and wing. This increase in rotor thrust is similar to "ground effect," where the thrust of a hovering rotor (at constant power) increases as it approaches the ground. The increase in thrust caused by the wing can be calculated by multiplying the expected increase in rotor thrust caused by the ground (Ref. 8) by the ratio of wing area to rotor disc area (14% here). For the present case, an increase in thrust of 2.9% is predicted using this technique. This value is very close to the measured thrust increase of 3%. From the data obtained in this test it appears that this method can be used to obtain reasonable estimates of the increase in rotor thrust caused by aerodynamic interactions with a wing. Note that the increase in thrust caused by the ground effect should be computed with the distance between the rotor and ground equal to the distance between the rotor and wing.

At a thrust coefficient representative of hover for the V-22 aircraft, (C_T = 0.016), the rotor thrust (at constant power) was reduced by 1.6% because of the aerodynamic interactions between the rotor and image plane. However, the configuration with the image plane and wing had essentially the same rotor performance as the configuration with the image plane alone. This was not expected because the wing caused an increase in the rotor performance with the image plane removed. Thus, the effect of the image plane on rotor performance was always negative, but the effect of the wing depended on whether the image plane was present.

A clue to the cause of this was provided by smoke flow visualization that was performed during testing with the wing and image plane installed. Figure 6 is a photograph that was taken during this flow visualization. The flow visualization revealed a large region of recirculating flow between the rotor, wing, and image plane. Some of the rotor wash was turned to a spanwise direction when it reached the wing (down in the photograph). When this spanwise flow encountered the image plane, it was turned to a direction parallel to the surface of the image plane and opposite the direction of the rotor wash (from right to left in the photograph). This flow separated from the image plane midway between the rotor and the left edge of the image plane, and was convected back into the rotor. Thus, a standing vortex existed in the corner formed by the wing and image plane, with the rotor driving the flow. The standing vortex could not be formed with the wing alone or the image plane alone. This standing vortex was similar to a vortex ring, and may have caused an increase in the induced power of the rotor. It is possible that the reduction in rotor performance caused by the standing vortex was approximately equal to the increase in rotor performance caused by the wing. This would explain the fact that the rotor performance with the image plane and wing was approximately equal to the rotor performance with the image plane alone. The computations described in Ref. 2 show a standing vortex similar to what was observed in the large-scale V-22 test. We believe that a similar standing vortex flow pattern exists on full-scale tilt rotor aircraft.

Large-Scale Rotor Downwash Velocities

A wake rake was used to measure the V-22 rotor downwash velocities with the wing removed. The rake was installed at the same location as the wing, about 0.42 rotor radii behind the rotor. The downwash velocities for four different thrust coefficients are presented in Fig. 7. The downwash velocities have been made nondimensional by dividing them by the ideal induced downwash velocity at the rotor disc, $V_H = \sqrt{T/2\rho A}$. No corrections have been made for ambient winds, which were typically less than 3% of the maximum downwash velocities.

At low thrust coefficients, the downwash velocities were higher on the inboard portions of the wake than on the outboard portions of the wake. This effect is reversed at the higher thrust coefficients, where the outboard portions of the wake have higher downwash velocities than the inboard region. This change in the wake downwash velocity distribution as the rotor thrust is increased causes a change in the wing download to rotor thrust ratio. This effect will be discussed further in the next section.

Large-Scale Wing Download

The V-22 wing download as a function of rotor thrust coefficient is shown in Fig. 8. Note that the wing download has been normalized by dividing it by the rotor thrust. The solid line is a least-squares polynomial curve fit of the data. These data were obtained with the wing flap at 67°. High oscillatory loads on the wing balances prevented testing at full-scale tip speeds, and all balance data were acquired at 62% of full-scale tip speed. The reduced tip speed probably had no effect on the nondimensional download results.

The download to thrust ratio (DL/T) in Fig. 8 decreases from 0.103 to 0.091 as the rotor thrust coefficient (C_T) increases from 0.004 to 0.020. The cause of this has been deduced from the flow visualization studies and the rotor downwash data.

Recall from the discussion on the effect of the wing and image plane on rotor performance that smoke flow visualization showed substantial spanwise flow on the wing, which was turned in a direction opposite that of the rotor downwash by the image plane. This flow is called a "fountain," and is common in VTOL aircraft flow fields. The change in momentum as this spanwise flow is turned at the image plane implies that this fountain contributes to the wing download.

Further information on the flow over the wing was provided by tufts installed on the wing surface. Figure 9 is a photograph of these tufts taken while the rotor was operating. The tufts at the wing tip (top of the wing in the photo) indicate that the flow in this region was essentially chordwise. The tufts at the wing root (bottom of the wing in the photo) indicate that the flow in this region was essentially spanwise.

The key to understanding the reduction in download as C_T was increased lies with the relative contributions to the total download of the chordwise flow at the wing tip and the spanwise flow at the wing root. The chordwise flow can be modeled as two-dimensional. To estimate the download of a wing section in this region, multiply the dynamic pressure of the rotor downwash impinging on the section by the drag coefficient of the airfoil at an angle of attack of -90°. A typical value for this drag coefficient would be 1.4, so the download of that section would be 1.4 times the dynamic pressure of the rotor downwash at the radius corresponding to the location of the wing section.

For the spanwise flow, the download is simply equal to the momentum flux of the fountain. This momentum flux is equal to the dynamic pressure of the fountain times the area of the fountain. Since the fountain is actually rotor downwash that has been turned 180°. by its interaction with the wing and image plane, the dynamic pressure in the fountain is approximately equal to the dynamic pressure of the rotor downwash that impinges on the wing in regions where the flow is predominantly spanwise.

It is possible to evaluate the relative contributions to the total download of the chordwise flow and the spanwise flow by using the ideas of the preceding paragraphs. The download per unit wing area is approximately 1.4 times the local rotor downwash dynamic pressure for chordwise flow, and approximately equal to the local rotor downwash dynamic pressure for spanwise flow.

The rotor downwash velocity data (Fig. 7) indicate that at low rotor thrust coefficients the dynamic pressure in inboard regions of the rotor wake (near the wing tip) is higher than the dynamic pressure in outboard regions of the wake (near the wing root). As the rotor thrust coefficient is increased, the dynamic pressure in the inboard regions of the wake becomes less than the dynamic pressure in the outboard regions of the wake. The inboard regions of the rotor wake contribute to the chordwise flow, and the outboard regions of the wake contribute to the spanwise flow. Therefore, the change in the downwash distribution with increasing C_T changes the relative contributions of the chordwise and spanwise flows to the total download. For a given area and dynamic pressure, chordwise flow produces more download than spanwise flow. Thus, as the rotor thrust coefficient is increased, more of the downwash dynamic pressure contributes to relatively more spanwise flow while less of the downwash dynamic pressure contributes to chordwise flow, and the download to thrust ratio decreases.

Large-Scale Wing Surface Pressures

Mean surface pressures on the large-scale wing upper and lower surfaces were measured at six chordwise rows. The surface pressures measured at two thrust coefficients with the wing flap set at 67° are shown in Fig. 10. The pressure data shown are the difference between the wing surface pressure and atmospheric pressure, and have been made nondimensional by dividing by the rotor disc loading. For clarity, the pressures measured on the wing flap are not shown. The loads on the flap were small compared with the loads on the rest of the wing, and the pressure data from the flap are therefore of less importance than those from the wing.

The large region of relatively constant negative pressure on the lower surface of the wing is characteristic of separated flow, and appears in the data acquired at all chordwise rows for all thrust coefficients. This large region of negative pressure makes a substantial contribution to the wing download. An even larger contribution to the download was provided by the positive pressure region on the upper surface. These pressures were of the same order as the rotor disc loading. The regions of high peak pressure on the upper surface at each thrust coefficient roughly correspond to the spanwise regions of high downwash dynamic pressure at that thrust coefficient. Thus, the rotor downwash was essentially stagnated by the wing over a large area of the wing's upper surface.

The pressure data support the explanation of the reduction in download with increasing thrust coefficient that was discussed in the previous section. If the pressures on the wing flap are neglected, then the download per unit span of the wing at a given row of pressure taps is proportional to the area inside the pressure distribution curves associated with that row of taps (Fig. 10). At the low thrust coefficient, the pressure distributions indicate that the download per unit span was higher on the inboard sections of the rotor disc than on the outboard sections of the rotor disc. Remember that the wing tip (inboard on the rotor disc) has predominantly chordwise flow, and the wing root (outboard on the rotor disc) has predominantly spanwise flow. Thus, at the low thrust coefficient, chordwise flow (at the wing tip) was making a larger contribution to the total download than spanwise flow (at the wing root). At the high thrust coefficient, the pressure distributions indicate that the regions of spanwise flow were making a larger contribution to the download than they were at the low thrust coefficient, and the regions of chordwise flow are making a smaller contribution to the total download at the high thrust coefficient than they were at the low thrust coefficient. Thus, the pressure distribution data support the explanation that was provided in the previous section concerning the reduction in download with increasing thrust coefficient.

Small-Scale Wing Download

The small-scale test was designed to complement the large-scale test by exploring the effect of various changes in the rotor/wing geometry on the rotor/wing aerodynamic interactions. Changes in the wing incidence angle, the distance between the rotor and wing, and the wing flap angle are examples of the configuration changes that were made in the small-scale test. The small-scale test was not intended to model any particular aircraft configuration, but to provide data on the trends of wing download with variations in the rotor/wing geometry. The small-scale investigation was also the first test to use boundary layer control in an effort to reduce wing download.

The rotor balance used in the small-scale test was not as accurate as the one used in the large-scale test. Consequently, the small interactions on the rotor caused by the presence of the wing could not be measured with high confidence. Therefore, this paper will concentrate on the wing download data obtained in the small-scale test, and will not address the interference on the small-scale rotor caused by the presence of the wing.

Effect of Rotor Thrust Coefficient on Download

The effect of rotor thrust coefficient on DL/T, as measured in the small-scale test, is shown in Fig. 11. Data are presented that were obtained with both of the wings used in the small-scale test, the NACA 23015 wing and the circulation control wing. The wing incidence angle was 0°, the rotor axis was at the center of the wings, and the separation between the rotor and wing was 0.4 rotor radii. The flap angle was zero on the NACA 23015 wing, and the boundary-layer control blowing was off on the circulation control wing. This was the baseline configuration for each wing. The download with these configurations was higher than the download measured in the large-scale test because the ratio of wing area to rotor disc area was higher in this small-scale test configuration.

The download to thrust ratio decreases with increasing thrust coefficient for both wings. This result is similar to what was found in the large-scale test, and the reason for it was probably the same: as the thrust coefficient increases, the region of maximum wake dynamic pressure moves outboard on the rotor disc. For this configuration, with the rotor axis at the center of the wing and no image plane, there is no fountain, and spanwise flow does not contribute to the download. Thus, the reduction in DL/T with increasing thrust coefficient should be even more pronounced here than in the large-scale test. Detailed flow visualization and wake velocity surveys were not made in the small-scale test, and these hypotheses were not verified to the extent that they were in the large-scale test.

Effect of Wing Flap Angle on Download

Wing flaps are used on the XV-15 and V-22 tilt rotor aircraft to reduce the wing download and to increase the wing lift in low speed flight. The effect of the flap angle on the small-scale wing download to thrust ratio is shown in Fig. 12. These data were obtained with the rotor axis at the center of the wing, the distance between the rotor and wing equal to 0.4 rotor radii, and 0° wing incidence angle. The download to thrust ratio was substantially decreased by increases in the flap angle, up to a flap angle of 75°. The download at 75° flap angle was about 30% less than the download at zero flap angle. For clarity, the data acquired with the flap angle set to 90° were not included in the figure. The download to thrust ratio with the flap set to 90° was approximately equal to the download to thrust ratio with the flap set at 60°.

The deflected wing flaps help to reduce the download in two different ways. First, the wing planform area was reduced by deflecting the flaps. For example, the wing planform was reduced 19% by deflecting the 25% chord plain flap 75°. Thus, if the wing section drag coefficient remained constant, the download would be reduced by 19% as well. Of course, the wing section drag coefficient does not remain constant, and was reduced by the deflection of the flap. This accounts for a further reduction in the download. For the case with a 25% chord plain flap deflected 75°, about two-thirds of the reduction in download relative to zero flap angle was caused by the reduction in wing planform area and one-third of the reduction in download was caused by the reduction in wing drag coefficient.

The fact that the download was higher with 90° of flap deflection than with 75° implies that the wing section drag coefficient was substantially higher at 90° flap deflection than it was at 75°. This was probably caused by flow separation over the flap at 90° flap angle that did not occur at the lower flap angles.

The data in Fig. 12 show that the download was reduced by 25% as the wing flap angle was increased from 0 to 60°. Unpublished XV-15 flight test data obtained from L. Schroers of Ames Research Center indicates that the download on the XV-15 is reduced by 32% as the flap angle is increased from 0 to 60°. The comparison between the two sets of data is favorable considering the differences between the rotors and wings in the two tests.

Effect of Wing Incidence Angle on Download

The wing incidence angle was varied in the test to simulate changes in the wing incidence angle on a compound helicopter or changes in the pylon angle on a tilt rotor aircraft in hovering flight. The effect of these incidence angle variations on the download to thrust ratio is shown in Figs. 13 and 14. The data shown in Fig. 13 were obtained by setting the flap angle to 60° and the distance between the rotor and wing to 0.4 rotor radii, and by placing the rotor axis at the center of the wing. Changing the wing incidence angle from the baseline of 0° to -8° caused an increase in the download of about 6%. Changing the wing incidence angle from 0° to +8° caused a decrease in the download of about 10%.

The incidence angle variations were repeated with the wing flap angle set to 0°, and with all other parameters held constant. The data obtained with this configuration are shown in Fig. 14. The incidence angle variations had a much smaller influence on the download with the flap set to 0° than they did with the flap set to 60°. Also, the trends of download with incidence angle variations were reversed. At 0° flap angle, changing the incidence angle from 0° to -8° caused a decrease in the download of about 3%, whereas the same change in incidence angle caused an increase in the download at 60° flap angle. Also, changing the incidence angle from 0° to +8° caused an increase in download at 0° flap angle, and the same change in incidence angle caused a decrease in the download at 60° flap angle. The cause of this is not presently understood.

Effect of Distance Between Rotor and Wing on Download

As the rotor wake convects away from the rotor disc, it contracts and the downwash velocities increase. Thus, it is to be expected that the distance between the wing and rotor will affect the rotor/wing aerodynamic interactions. The effect of the distance between the rotor and wing on the wing download is shown in Fig. 15. These data were obtained by setting the wing at 0° incidence angle and 60° flap deflection, and by placing the rotor axis at the center of the wing. The span of the wing was 0.75 rotor radii, and it was fully immersed in the rotor wake at all times.

The wing download was increased by about 9% as the distance between the rotor and wing was decreased from 0.4 to 0.217 rotor radii. The wing download was decreased about 9% as the distance between the rotor and the wing was increased from 0.4 to 0.655 rotor radii. The mean rotor downwash velocities should be smaller near the rotor than they are in the fully developed rotor wake (from momentum theory). This would imply lower download as the wing is moved near the rotor, which is the opposite of what was observed. The higher download near the rotor is caused by large periodic airloads (at the blade passage frequency) that diminish as the wing moves farther away from the rotor (Ref. 3). Thus, the rotor/wing aerodynamic interactions involve complex phenomena, and the wing cannot be viewed simply as a body immersed in a uniform free stream with a velocity equal to the local rotor downwash velocity.

Effect of Rotor Position on Download

All of the small-scale data presented so far were obtained with the rotor axis at the center of the wing (representative of a compound helicopter). Data were also acquired with the rotor axis located at the wing tip (representative of a tilt rotor aircraft), and all of the parameter changes previously discussed were made in both configurations. In general, the trends and magnitudes of the effects previously discussed were not changed significantly when the rotor axis was located at the wing tip instead of the center of the wing. Therefore, the effect on the hover download of variations in rotor thrust coefficient, wing flap angle, wing incidence angle, and distance between the rotor and wing will not be discussed for data obtained with the rotor axis at the wing tip.

Most of the data acquired with the rotor axis at the wing tip were obtained with an image plane installed on the wing to simulate the presence of a second rotor and wing on a tilt rotor aircraft. This image plane was located 1.29 rotor radii from the rotor axis and was 0.86 rotor radii square. Note that the location of the image plane relative to the rotor was similar in the large- and small-scale tests, but the image plane used in the small-scale test was much smaller, relative to the rotor, than the image plane used in the large-scale test. Also, the large-scale test configuration included a simulated rotor/fuselage fairing. Some data were acquired with the image plane removed, and the effect of the image plane on the download will be discussed in a later section.

The effect of rotor position on wing download for two different flap angles is shown in Fig. 16. These data were obtained with $z/R = 0.4$, 0° wing incidence angle, and the image plane on when the rotor axis was at the wing tip. For both flap angles, the download with the rotor axis at the wing tip was about two-thirds of the download with the rotor axis at the center of the wing. All of the wing was within the area of the rotor disc when the rotor axis was at the center of the wing, while only two-thirds of the wing was within the rotor disc when the rotor axis was at the wing tip. Thus, it appears that the reduction of download was caused by less of the wing being in the rotor wake when the rotor axis was at the wing tip. Furthermore, the data indicate that the download divided by the ratio of wing area to rotor disc area is approximately constant.

Effect of Rotor Rotation Direction on Download

Most of the testing with the rotor axis at the wing tip was accomplished with the rotor rotation going from the wing leading edge to the wing trailing edge. This is the rotation direction that is used on both the XV-15 and V-22 tilt rotor aircraft. However, data were acquired at 60 and 75° flap angles with the rotor turning in the opposite direction, with the blades moving from the wing trailing edge to the leading edge. Figure 17 shows the effect of rotor rotation direction on the wing download with the flap set to 75°. These data were obtained with 0° wing incidence angle, $z/R = 0.4$, and the image plane on. The download measured when the rotor was rotating from trailing edge to leading edge was about 20% less than the download measured with the normal rotor rotation direction. Reversing the normal rotor rotation direction reduced the download with the flap angle set to 60°, too. However, the reduction in download with 60° flap angle was only about 12%, which was substantially less than the download reduction with 75° flap angle. This indicates that the changes in download with rotor rotation direction are partly caused by changes in the flow over the deflected flap. Perhaps separation on the upper surface of the flap at the higher flap deflections is delayed when the rotor wake swirl velocity goes from trailing edge to leading edge, and the download is thereby reduced.

Effect of Image Plane on Download

All of the data shown so far with the rotor axis at the wing tip were obtained with the image plane installed. It was demonstrated in the large-scale test that the fountain which forms on the wing upper surface at the centerline of a tilt rotor aircraft contributes to the download. Therefore, some data were acquired in the small-scale test with the image plane removed in an effort to quantify the magnitude of this effect for the small-scale test configuration. Figure 18 shows the effect of the image plane on the download with $z/R = 0.4$, 0° wing incidence angle, and 60° flap angle. The image plane had essentially no effect on the download with this configuration. Smoke flow visualization revealed that the image plane was having very little effect on the rotor/wing flow field. The recirculating rotor/wing/image plane flow field observed in the large-scale test was not observed in the small-scale test. It was clear from the flow visualization that the image plane was much too small to have a significant effect, and therefore did not provide a realistic simulation of a tilt rotor aircraft.

Data were also acquired with the image plane off and the distance between the rotor and wing equal to 0.217 rotor radii. The data obtained with this configuration are shown in Fig. 19. As before, the wing incidence angle was 0° and the flap angle was 60°. At this rotor/wing separation distance, the image plane did have a significant effect on the download. The download with the image plane on was about 17% higher than the download when the image plane was off. This increase in the download is caused by the fountain at the junction between the wing and image plane (and at the centerline of a tilt rotor aircraft) that was previously discussed. Apparently, the size of the image plane relative to the distance between the rotor and wing is just as important as the size of the image plane relative to the rotor. In any case, if it is not possible to use two rotors and wings, then the largest image plane that is practical should be used in future investigations.

Download Reduction Using Boundary Layer Control

In addition to the conventional flapped wing, a second wing was tested that used boundary-layer control in an effort to reduce the download. This wing had slots for upper surface boundary-layer control blowing at the wing leading and trailing edges (Fig. 3). The jets of air from these slots should remain attached to the airfoil surface because of the Coanda effect. If this high energy boundary layer, caused by the blowing, delays or prevents the rotor downwash from separating from the wing leading and trailing edges, then the download will be reduced.

Effect of Blowing Pressure on Download

The effect of the blowing pressure ratio on the download of the circulation control wing is shown in Fig. 20. The pressure ratio is defined as the pressure in the blowing slot supply plenum, P_p, divided by atmospheric pressure, P_{atm}. The data in these figures were acquired with the wing at 0° incidence angle, $z/R = 0.4$, and with the rotor axis at the center of the wing. The data shown in Fig. 20(a) were obtained with the ratio of slot height to wing chord equal to 0.0014, and in Fig. 20(b) the slot height to wing chord ratio was 0.0010.

Figures 20(a) and 20(b) show that the download is steadily reduced by boundary-layer blowing as the blowing pressure ratio is increased to 1.06. As the pressure ratio is increased past 1.06, there is little further reduction in the download. The reduction in download caused by the boundary-layer control blowing is greatest at low thrust coefficients, although there is little effect of thrust coefficient on the reduction in download at thrust coefficients above 0.007 (Fig. 20 (b)). The ratio of the velocity in the boundary-layer control blowing to the rotor downwash velocity is higher at low thrust coefficients than at high thrust coefficients, and this accounts for the greater reduction in download at low thrust coefficients. The reduction in download caused by boundary-layer control blowing ranges from 54% at a thrust coefficient of 0.003 to 25% at a thrust coefficient of 0.009.

Effect of Blowing Slot Height on Download

For a given pressure ratio, the mass flow of the boundary-layer control blowing increases linearly with the blowing slot height. The weight of the air supply system, and the power required to operate it, are increased as the blowing mass flow is increased. Therefore, it is desirable to use the minimum slot height that will effectively reduce the download.

The effect of the blowing slot height on the download is shown in Fig. 21. These data were obtained with the wing at 0° incidence angle, z/R = 0.4, and with the rotor axis at the center of the wing. The slot heights tested ranged from 0.1% to 0.21% of the wing chord. The data shown in Fig. 21 indicate that the slot height had little effect on the download. There was some reduction in the download as the slot height was increased from 0.1% to 0.21% of the wing chord, but the small reduction in download does not justify the 110% increase in mass flow associated with the larger slot height. Since the slot height does not have a significant effect on the download, future investigations of download reduction using boundary-layer control blowing should concentrate on slot heights of 0.1% of the wing chord or less, since the lower mass flow associated with the lower slot heights implies lower weight and less power for the wing air supply system.

The fact that the slot height has little effect on the download has some interesting implications. Apparently, the mass flow and momentum of the blowing jet are not important parameters. This is in contrast to what has been observed in other applications of the circulation control concept. Normally, the momentum of the blowing jet is of fundamental importance. Also, the fact that the download is primarily controlled by the blowing pressure ratio means that the velocity of the blowing jet is an important parameter, and the ratio of the blowing jet velocity to the rotor downwash velocity is relatively unimportant, especially at high thrust coefficients.

Comparison of Download with One and Two Blowing Slots

The wings on the XV-15 and V-22 tilt rotor aircraft have flaps at the trailing edge, and it would be difficult to modify these aircraft to utilize boundary-layer control blowing at the trailing edge. However, it would not be difficult to incorporate boundary-layer control blowing at the leading edges of these aircraft, and it is therefore interesting to evaluate the effectiveness of the boundary-layer control blowing when it is only applied to the wing leading edge.

A comparison of the download measured with one and two blowing slots is shown in Fig. 22. These data were obtained with the wing at 0° incidence angle, z/R = 0.4, the rotor thrust coefficient equal to 0.0086, and the rotor axis at the center of the wing. The download is reduced about 26% when both slots were blowing, and about 17% when only one slot was blowing. Thus, 65% of the reduction in download obtained by blowing with two slots is obtained by blowing with only one slot. The cause of this behavior is not known. In any case, it is clear that significant reductions in download can be obtained by blowing at the wing leading edge only and by continuing to use a conventional flap at the wing trailing edge. The data obtained in this test indicate that a wing with the combination of a flap and leading edge blowing will have significantly less download than a wing with a flap alone, or a wing with blowing at the leading and trailing edges. Therefore, it should be possible to evaluate this download reduction concept on existing tilt rotor aircraft without extensive modifications.

Circulation Control Wing Surface Pressures

Figures 23(a) and 23(b) show the wing surface pressures measured on the circulation control wing with the boundary-layer control blowing off and on, respectively. These data were obtained with the wing incidence angle equal to 0°, z/R = 0.4, the slot height equal to 0.1% of the wing chord, and the rotor axis at the center of the wing. The wing surface pressures have been made nondimensional by dividing by the disc loading.

The data obtained with the blowing off (Fig. 23(a)) exhibit many features that are similar to the data from the large-scale wing previously discussed and presented (for example, Fig. 10(c)). There is a large region on the upper surface of the wing where the pressure is approximately equal to the rotor disc loading, which indicates that the rotor downwash has been stagnated. The entire lower surface of the wing has constant, slightly negative pressure, which is characteristic of separated flow. The rotor downwash has separated from the wing at the leading and trailing edges. The asymmetry in the pressure distribution is probably caused by the swirl in the rotor wake, which is from the wing leading edge to the wing trailing edge at this wing station.

By comparing the data obtained with the boundary-layer control blowing on (Fig. 23(b)) with that obtained with the blowing off (Fig. 23(a)), the aerodynamic phenomena responsible for the reduction in download can be determined. The region of stagnated flow exists on the upper surface of the wing whether the blowing is on or off, however this region is smaller when the blowing is on. In fact, there is a large region of negative pressure on the wing upper surface near the leading edge when the blowing is on. This negative pressure region extends well aft of the location of the blowing slot, which is located at 3% of the wing chord. This indicates that the blowing jet has entrained the rotor downwash, thereby reducing the size of the region of stagnated flow on the wing upper surface. The large region of negative pressure on the upper surface of the wing does not exist at the wing trailing edge. This phenomenon was probably caused by the asymmetry induced by the swirl velocity in the rotor wake.

The boundary-layer control blowing was originally intended to reduce the download by delaying or preventing the rotor wake from separating from the wing leading and trailing edges. The degree to which the blowing has accomplished this objective can be evaluated by comparing the pressures on the wing lower surface when the blowing is on and off. Figures 23(a) and 23(b) show that the pressure on the lower surface of the wing was only slightly less negative when the blowing was on than when it was off. Thus, the boundary layer control blowing has had little success in preventing the rotor downwash from separating from the wing leading and trailing edges.

With the boundary-layer control blowing on, the wing download was reduced by negative pressure on the wing upper surface and an increase in pressure on the lower surface. The relative magnitudes of these effects were evaluated by integrating the wing surface pressure data. The result was that the negative pressure on the upper surface of the wing was responsible for about two-thirds of the total reduction in download, and the increased pressure on the lower surface caused about one-third of the total reduction in download.

Careful study of the pressure distribution on the wing when the blowing was off reveals that the attempt to reduce the download by preventing flow separation at the wing leading and trailing edges may have been a mistake. Most of the download is caused by the large region of stagnated flow on the upper surface of the wing, and relatively little download is caused by the negative pressure on the lower surface (caused by flow separation). It seems unlikely that the pressure on the lower surface of the wing could be increased above atmospheric, so the potential for reducing the download by increasing the lower surface pressure is small. There is more potential for reducing the download by minimizing the size of the stagnated flow region on the upper surface of the wing. The boundary layer control blowing caused a substantial reduction in the pressure on the wing upper surface well aft of the blowing slot, which accounts for most of the download reduction caused by the blowing. Future investigations of download reduction using this boundary layer control concept should investigate blowing slot locations on the upper surface of the wing that are farther from the leading or trailing edge than the 3% of chord that was tested here. It may be possible to increase the size of the negative pressure region on the wing upper surface caused by the blowing, and thereby obtain further reductions in the download.

Wing Download Predictions

A semi-empirical theory has been developed to predict the download on a wing immersed in the wake of a hovering rotor. This theory relies heavily on the flow visualization results and rotor downwash measurements that were obtained in the large-scale test. A major objective during the development of the theory was to make it computationally efficient, so that it would be practical to incorporate the method into a comprehensive rotorcraft analysis program or a preliminary design code.

In plan view, the wing is divided into a number of quadrilateral panels. There are N chordwise rows, and M spanwise rows, for a total of NxM panels. Typically, 20 panels in the chordwise direction and 50 panels in the spanwise direction were used. The panels cover the actual wing planform only, and as the wing flap is deflected the size of the wing planform is reduced.

The mean dynamic pressure in the rotor wake as a function of rotor radius and thrust coefficient is obtained from experimental data, or from some other analysis. It is important that the wake dynamic pressure distribution be measured or computed at the same distance from the rotor disc as the wing location. In addition to the wake dynamic pressure measurements previously described in this paper, the data of Ref. 9 were also used in this investigation.

The analysis assumes that the rotor downwash is turned by the wing from an axial direction to a direction parallel to the wing surface, without any losses. In the analysis, the direction of the flow along the wing surface is specified based on the observed flow directions in the large-scale V-22 rotor/wing test. The flow on the wing is assumed to be chordwise for regions on the wing located less than a specified distance from the rotor axis, R_c. For regions on the wing farther from the rotor axis than R_c, the flow direction is along a ray from a point on the wing leading edge to the point on the wing surface in question (see Fig. 24). This point on the wing leading edge is located at the intersection of the wing leading edge with a circle whose center is at the rotor axis, and whose radius is R_c.

R_c is a function of the rotor thrust coefficient. For thrust coefficients of 0.006 or less, R_c is equal to 0.4 rotor radii. R_c increases linearly from 0.4 to 0.6 rotor radii as the thrust coefficient is increased from 0.006 to 0.014. For thrust coefficients above 0.014, R_c is equal to 0.6. These variations in R_c are intended to model the increased size of the chordwise flow region as the region of maximum dynamic pressure in the rotor wake moves outboard with increasing thrust coefficient. The flow directions assumed agree reasonably well with those observed in the large-scale V-22 test, and were easy to implement into the analysis. It is expected that R_c will be affected by the details of a specific configuration, such as rotor blade taper and twist, wing dihedral, etc.

After the direction of the flow over a given panel is determined, the magnitude of the flow is found from the rotor downwash characteristics. The downwash characteristics are determined analytically or measured experimentally without the wing in the rotor wake. Then the flow over each panel is divided into spanwise and chordwise components.

For a compound helicopter, the spanwise flow spills off the tip of the wing and does not contribute to the download. However, for a tilt rotor, the spanwise flow from each wing meets in the center of the aircraft and forms a fountain which adds to the total download. Therefore, in the analysis it is assumed that for tilt rotor configurations all of the spanwise flow is turned upward at the center of the aircraft, and all of the momentum of this flow contributes to the download. The download caused by the spanwise flow is found by multiplying the dynamic pressure of the spanwise flow over each panel by that panel's area. This quantity is summed for all panels on the wing, and the sum is equal to the download caused by spanwise flow.

The dynamic pressure of the chordwise flow over each panel is multiplied by the area of the panel, and this quantity (the "loading") is summed for each chordwise row. Each chordwise row of panels has a two-dimensional drag coefficient based on the airfoil geometry and flap deflection. These two-dimensional drag coefficients can be obtained from a wind tunnel test of the airfoil of interest at -90° angle of attack. For the computations described herein, the wind tunnel data of Ref. 1 were used. Finally, the drag coefficient of a row is multiplied by the loading to find the download caused by the chordwise flow. Thus, the download on each chordwise row is:

$$\text{Download} = C_D \sum_{i=1}^{N} [(\text{area of panel})_i \times (\text{dynamic pressure of chordwise flow at panel})_i]$$

The total download on the wing caused by the chordwise flow is found by summing the download on each chordwise row. The total download on the wing is then obtained by adding the download caused by spanwise flow to the download caused by chordwise flow.

This analysis is very efficient, requiring only modest amounts of computer time. A typical case with 1000 panels requires about 5 sec of CPU time on a VAX 11-780 computer system.

Comparison of Theoretical Predictions with Test Data

A comparison of the predicted download on the V-22 wing with the large-scale test data is shown in Fig. 25. The correlation is excellent for this case. This is not unexpected in light of the fact that the analysis was developed using flow visualization and rotor wake velocity data obtained in this test.

A comparison of the predicted download with XV-15 flight test data is shown in Fig. 26. The unpublished flight test data were obtained from L. Schroers of Ames Research Center. The download was not directly measured in the flight tests, but was deduced based on analysis of the rotor torque and aircraft gross weight. The rotor thrust was computed from the rotor torque data obtained in the flight test and the isolated rotor hover performance data of Ref. 10. The computed rotor thrust was reduced by 1.6% to account for rotor/wing and rotor/rotor interference. The download is the difference between the total rotor thrust and the aircraft gross weight.

The predicted download is less than the measured download for all flap angles. At the lower flap angles, the download is underpredicted by about 20%. The correlation improves as the flap angle is increased, and the error is only 8% at 60° flap angle. The flow directions on the wing surface were specified in the theory based on flow visualization conducted in the large-scale V-22 test. This visualization was conducted with the wing flap set to 67°. Perhaps the surface flow on the wing changes as the wing flap angle is changed. This could account for the good correlation at high flap angles, and the poor correlation at low flap angles.

Conclusions

Large-scale and small-scale experimental investigations of rotor/wing aerodynamic interactions in hover were described. Comprehensive results were obtained, covering a wide range of parameters and rotor/wing geometries. A semi-empirical theory was developed to predict wing download based on the flow visualization and rotor downwash results of the large-scale experiment. The theory correlates well with available large-scale tilt rotor download data. Some important conclusions that were drawn from this investigation were:

1. The thrust of the large-scale V-22 rotor (at constant power) was increased by 3% when the wing was installed. When the image plane was installed along with the wing, simulating the presence of a second wing and rotor on a tilt rotor aircraft, the rotor thrust was reduced 1.6% from the isolated rotor condition. This adverse interference was caused by a standing vortex in the rotor/wing/image plane flow field.

2. The ratio of wing download to rotor thrust was higher at low rotor thrust coefficients than at high rotor thrust coefficients. This was observed in the large-scale and small-scale tests. The change in download to thrust ratio was caused by changes in the rotor downwash velocity distribution as the thrust coefficient was increased.

3. Wing incidence angle, the distance between the rotor and wing, the wing flap angle, and the direction of rotor rotation all had a significant effect on the wing download.

4. Wing download was reduced by boundary-layer control blowing. The reduction in download ranged from 54% at low rotor thrust coefficients to 25% at high rotor thrust coefficients. The blowing slot height had little effect on the download. The surface pressure data indicate that upper surface blowing has a higher potential for reducing the download than lower surface blowing.

5. Using the optimum combination of trailing edge flap angle, leading edge blowing, and rotor rotation direction, the download on the XV-15 Tilt Rotor Research Aircraft could be reduced from 12% to 8% of the rotor thrust.

6. A theory to predict wing download was developed using the flow visualization and rotor wake velocity data obtained in the large-scale test. Theoretical predictions correlate well with large-scale tilt rotor download data obtained in the large-scale V-22 test and in flight tests of the XV-15 aircraft.

References

1. McCroskey, W. J., Spalart, P., Laub, G. H., and Maisel, M. D., "Airloads on Bluff Bodies, with Application to the Rotor-Induced Downloads on Tilt-Rotor Aircraft," Vertica, 9, (1), 1985.

2. McVeigh, M. A., "The V-22 Tilt Rotor Large-Scale Rotor Performance/Wing Download Test and Comparison with Theory," presented at the 11th European Rotorcraft Forum, London, England, Sept. 1985.

3. Makofski, R. A., and Menkick, G. A., "Investigation of Vertical Drag and Periodic Airloads Acting on Flat Panels in a Rotor Slipstream," NACA TN 3900, Dec. 1956.

4. McKee, J. W., and Naeseth, R. L., "Experimental Investigation of the Drag of Flat Plates and Cylinders in the Slipstream of a Hovering Rotor," NACA TN 4239, Apr. 1958.

5. Marr, R. L., Ford, D. G., and Ferguson, S. W., "Analysis of the Wind Tunnel Test of a Tilt Rotor Powered Force Model," NASA CR 137529, June 1974.

6. Clark, D. R., and McVeigh, M. A., "Analysis of the Wake Dynamics of a Typical Tilt-Rotor Configuration in Transition Flight," presented at the 11th European Rotorcraft Forum, London, England, Sept. 1985.

7. Felker, F. F., Maisel, M. D., and Betzina, M. D., "Full-Scale Tilt-Rotor Hover Performance," Journal of the American Helicopter Society, Apr. 1986.

8. Keys, C. N., "Rotary-Wing Aerodynamics: Vol. II - Performance Prediction of Helicopters," NASA CR 3083, Jan. 1979.

9. Felker, F. F., Young, L. A., and Signor, D. B., "Performance and Loads Data from a Hover Test of a Full-Scale Advanced Technology XV-15 Rotor," NASA TM 86854, Jan. 1986.

10. Felker, F. F., Betzina, M. D., and Signor, D. B., "Performance and Loads Data from a Hover Test of a Full-Scale XV-15 Rotor," NASA TM 86833, Nov. 1985.

TABLE 1.- LARGE-SCALE ROTOR CHARACTERISTICS

Radius	3.81 m
Chord	tapered, 0.454 m at .75R
Airfoils	Bell XN09/XN12/XN18/XN28
Number of blades	3
Twist	-48° nonlinear
Solidity	0.1138

TABLE 2.- LARGE-SCALE WING CHARACTERISTICS

Span (to image plane)	4.75 m
Chord	1.76 m
Thickness ratio	0.23
Twist	0°
Dihedral	6°
Airfoil	Bell A821201
Locations of Pressure Taps, %R	16, 30, 50, 70, 83, 90

TABLE 3.- SMALL-SCALE ROTOR CHARACTERISTICS

Radius	1.067 m
Chord	0.0629 m
Airfoils	SC1095/SC1095R8
Number of blades	4
Twist	-10° linear
Solidity	0.0751

TABLE 4.- SMALL-SCALE WING CHARACTERISTICS

	Circ Control	23015
Span	1.60 m	1.60 m
Chord, c	0.447 m	0.447 m
Thickness, t/c	0.2125	0.15
Twist	0	0
Dihedral	0	0
Camber, y/c	0.05	0.0184
Slot locations, x/c	0.03, 0.97	---
Leading edge radius, % chord	5.25	2.48
Locations of Pressure Taps, % semispan	13, 27, 53, 80, 93	

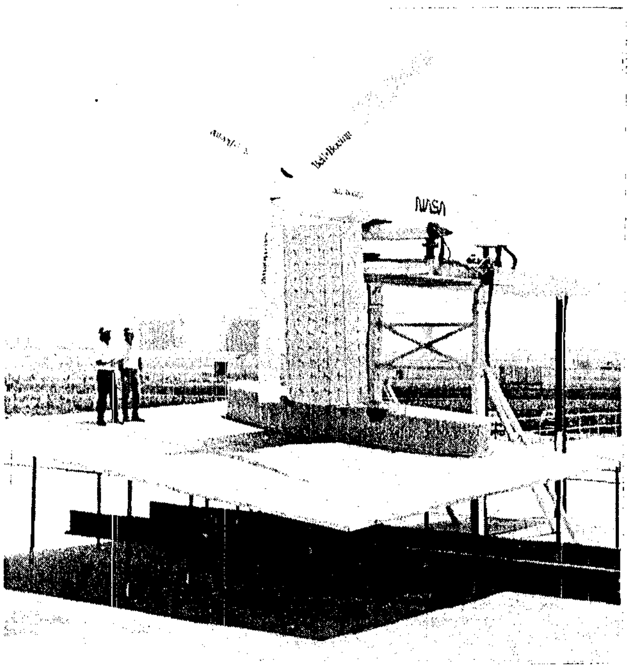

Figure 1. 0.658-Scale, V-22 Rotor and Wing.

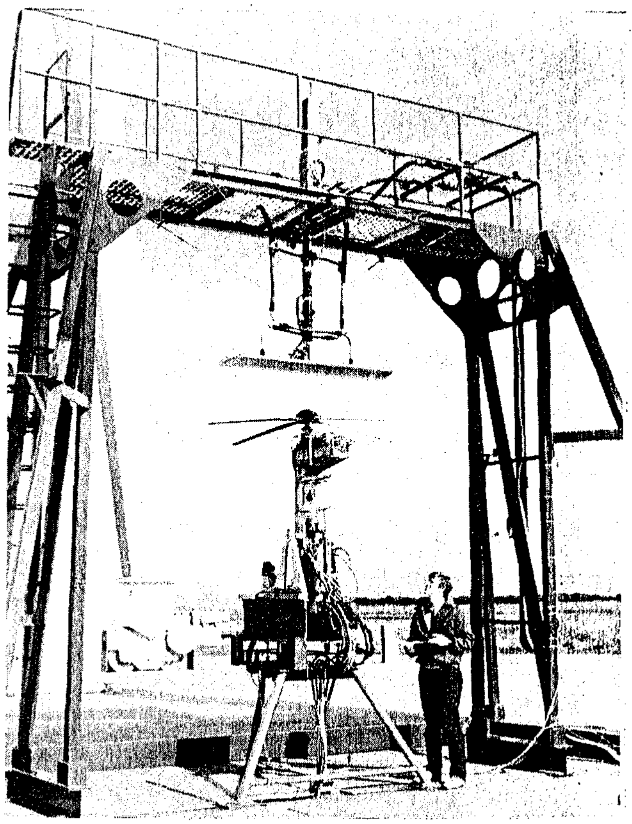

Figure 2. NASA Ames Rotor Test Rig with Circulation Control Wing.

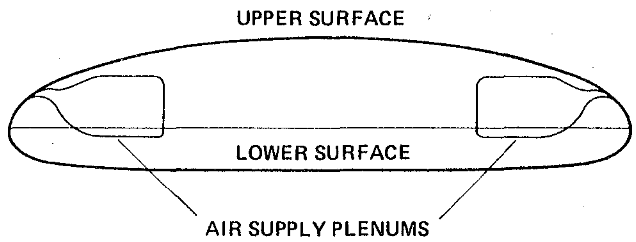

Figure 3. Circulation Control Wing Airfoil Section.

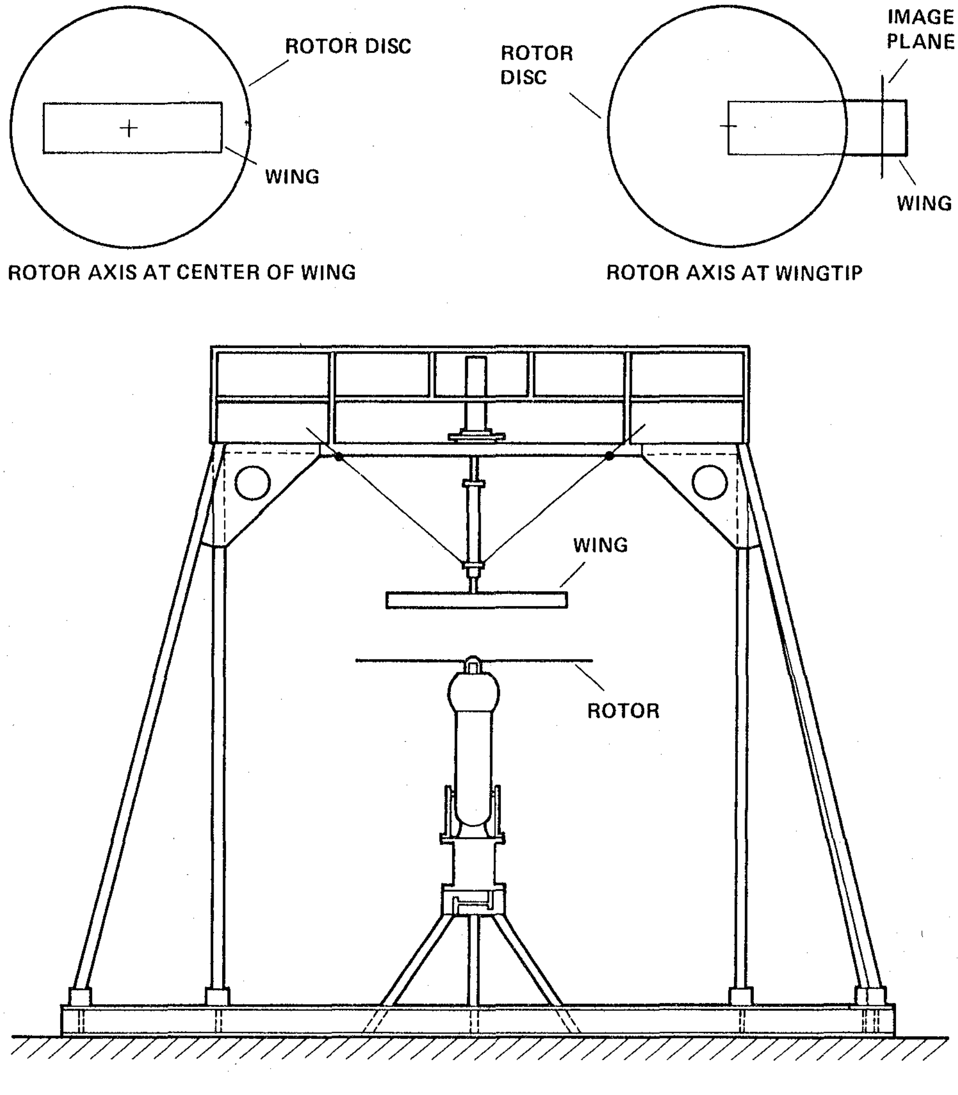

Figure 4. Small-Scale Test Configuration.

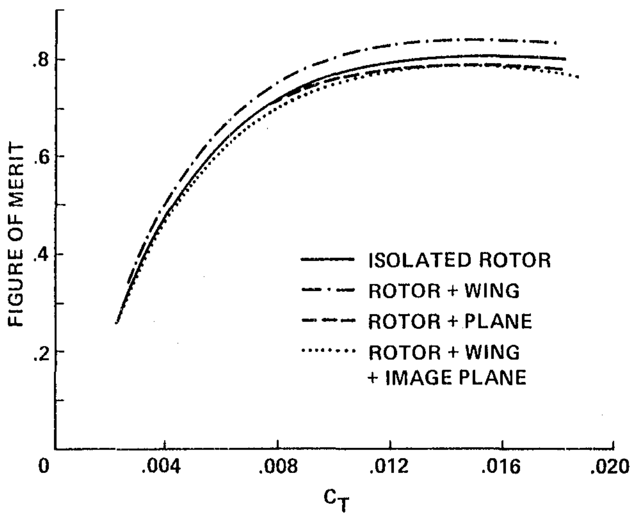

Figure 5. Large-Scale Rotor Performance.

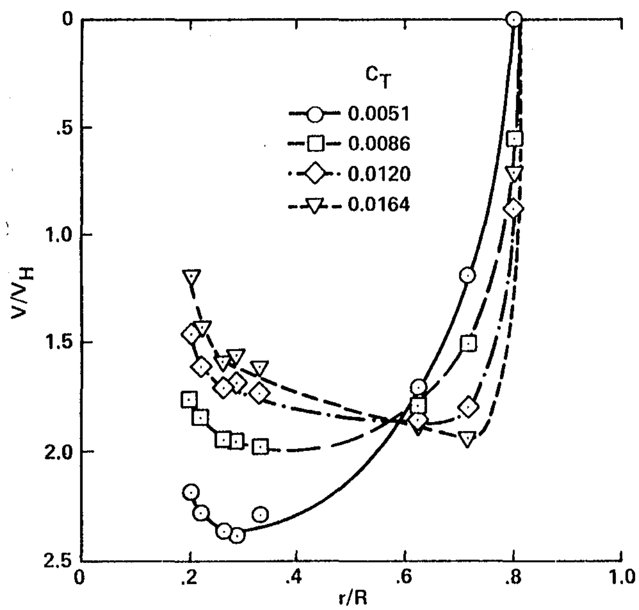

Figure 7. V-22 Rotor Downwash Velocities.

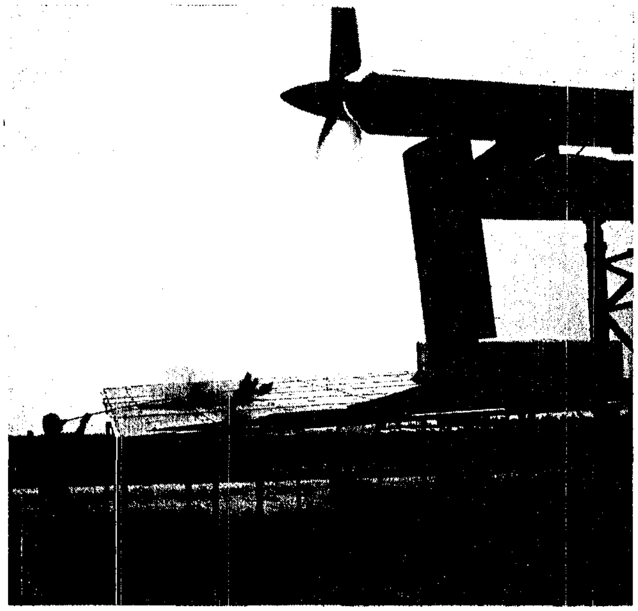

Figure 6. Flow Visualization of Rotor/Wing/Image Plane Flow Field.

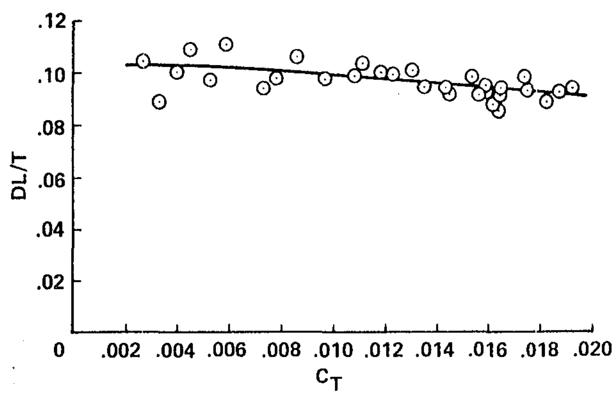

Figure 8. V-22 Wing Download.

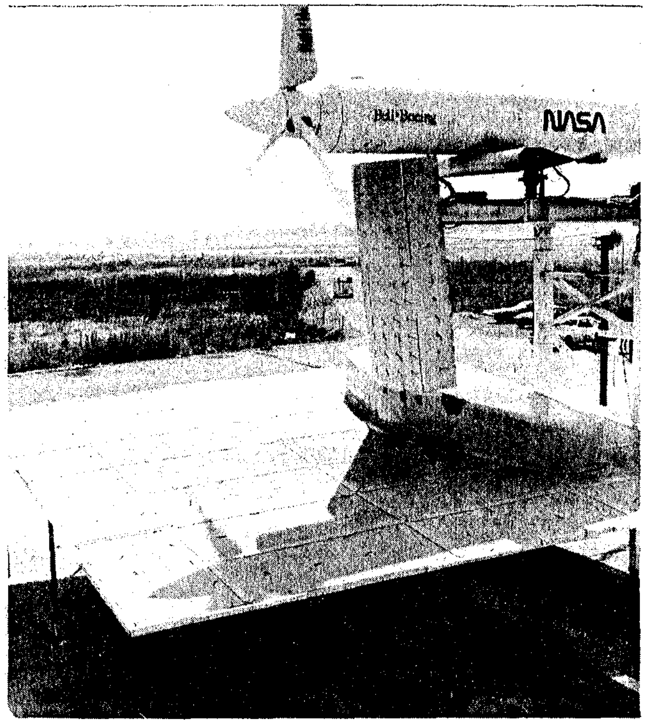

Figure 9. Wing Surface Flow Visualization with Tufts.

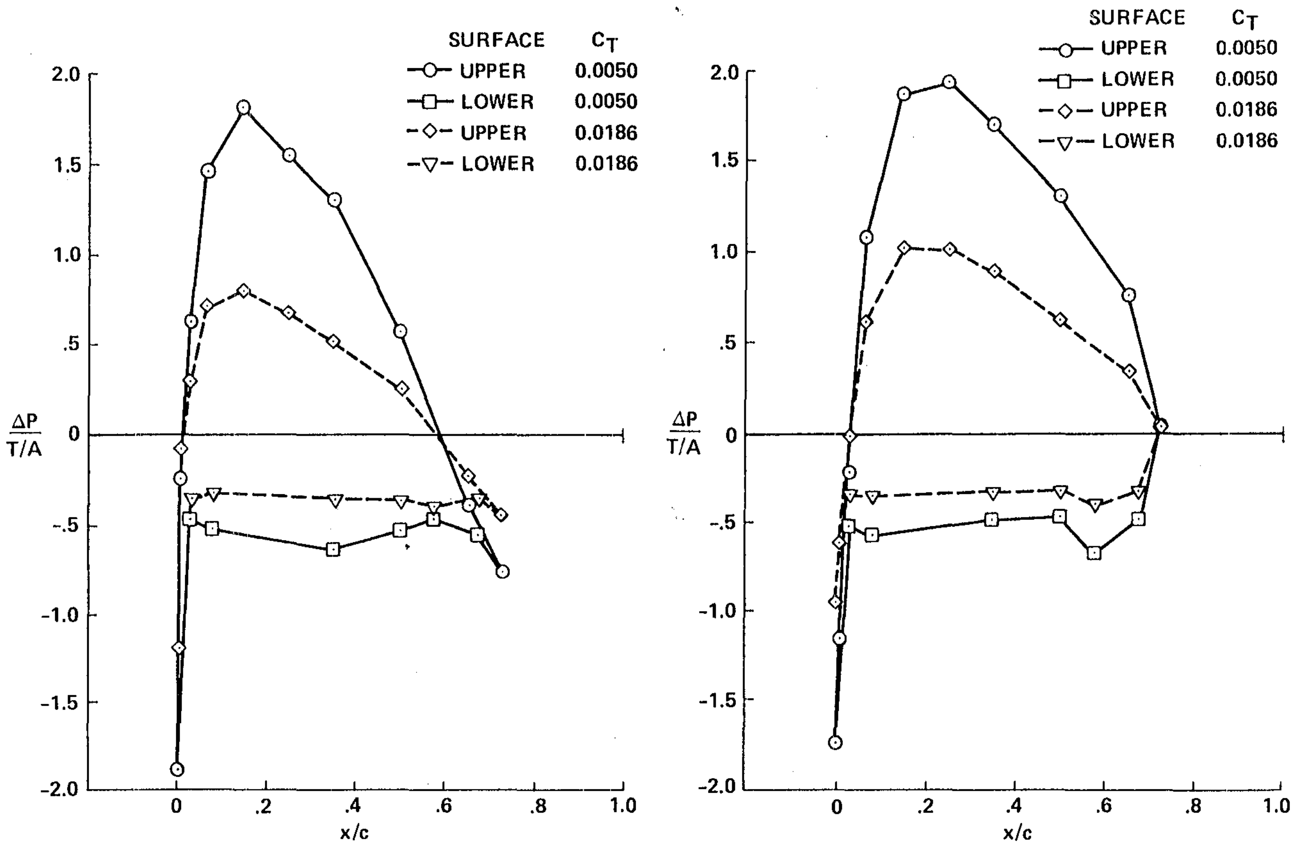

(a) 0.16 R.

(b) 0.30 R.

Figure 10. V-22 Wing Surface Pressures.

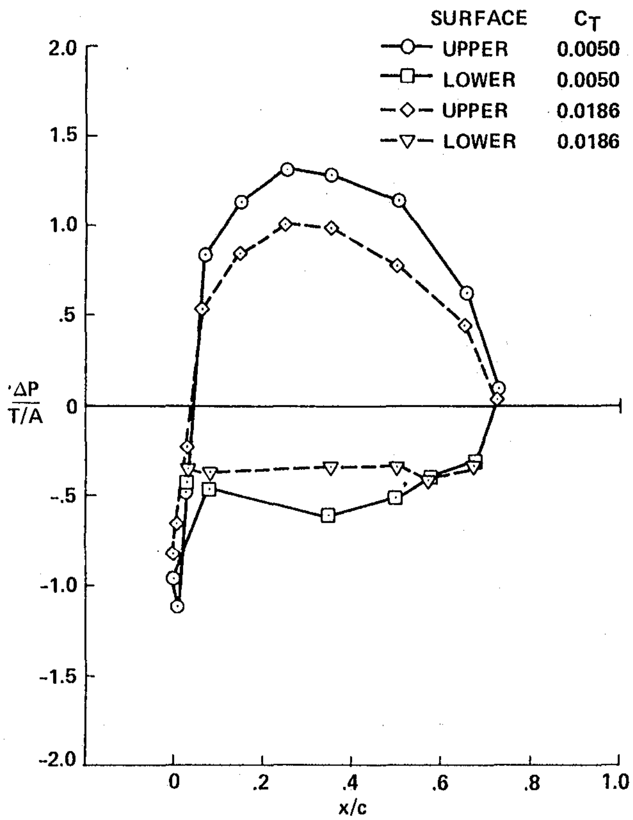

(c) 0.50 R.

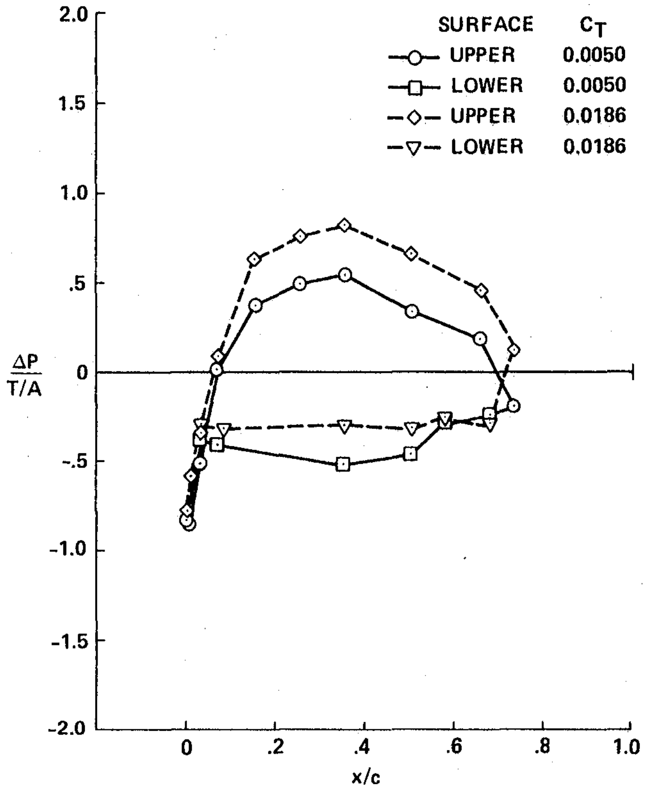

(d) 0.70 R.

Figure 10. Continued.

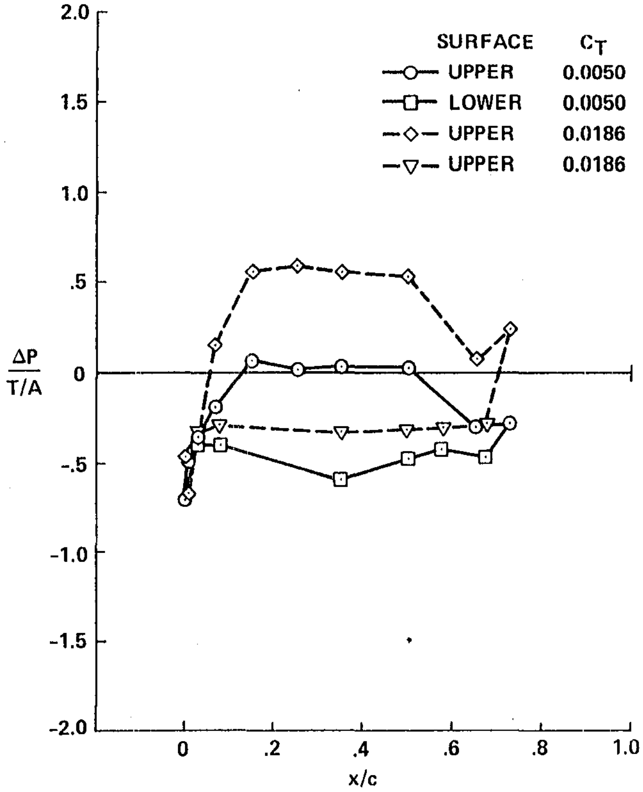

(e) 0.83 R.

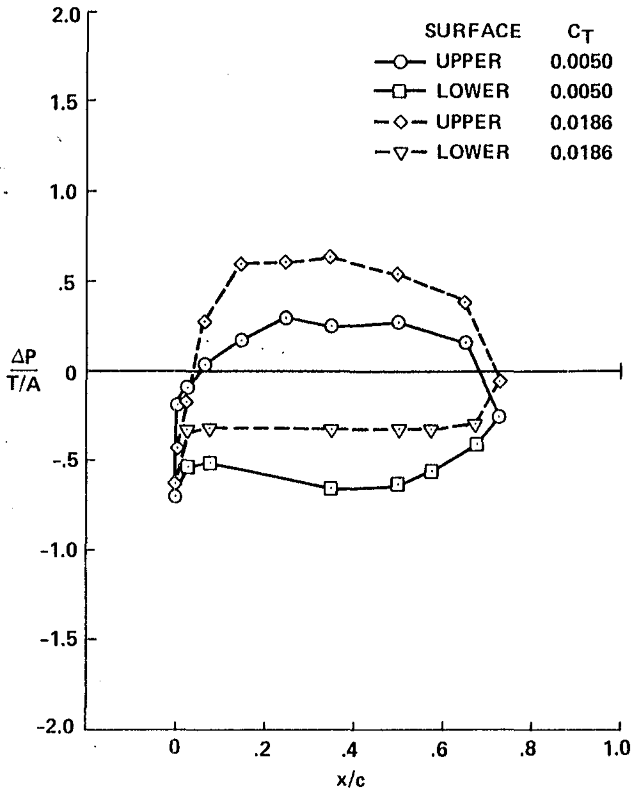

(f) 0.90 R.

Figure 10. Concluded.

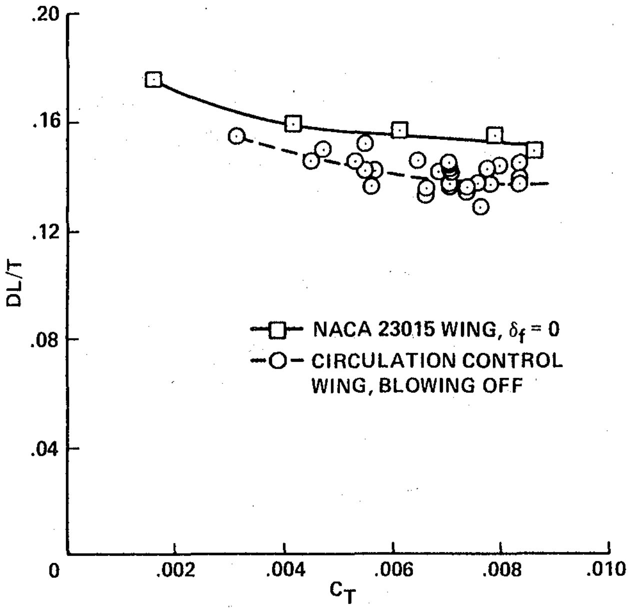

Figure 11. Effect of Rotor Thrust on Small-Scale Wing Download.

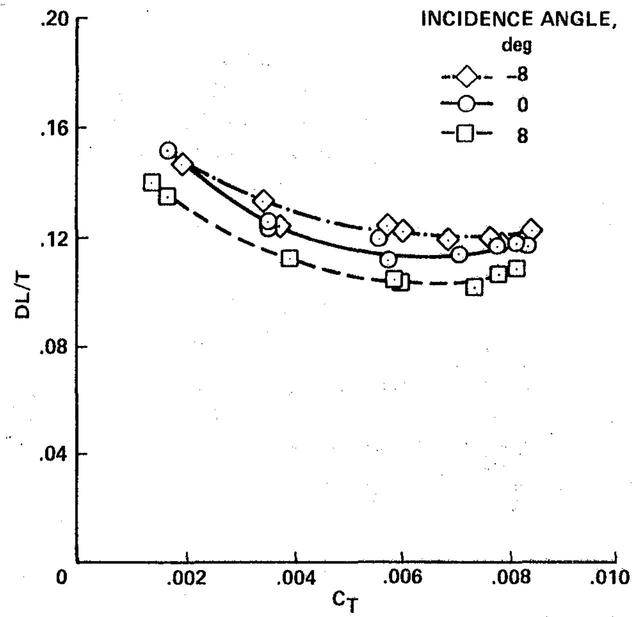

Figure 13. Effect of Wing Incidence Angle on Small-Scale Wing Download - δ_F = 60°.

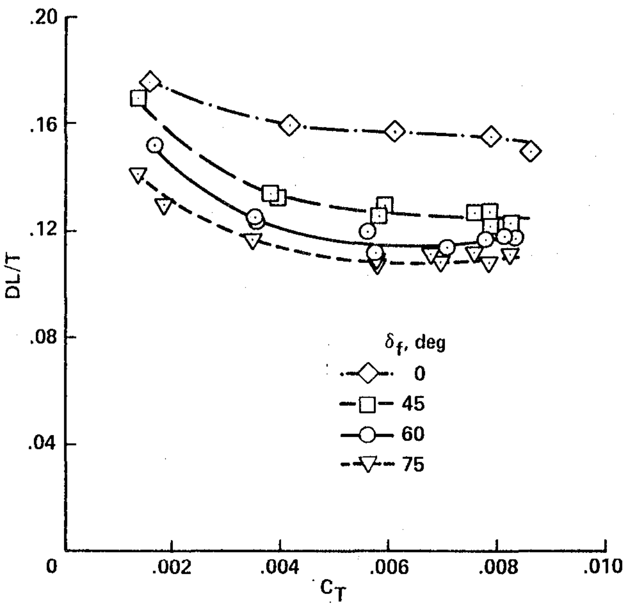

Figure 12. Effect of Wing Flap Angle on Small-Scale Wing Download.

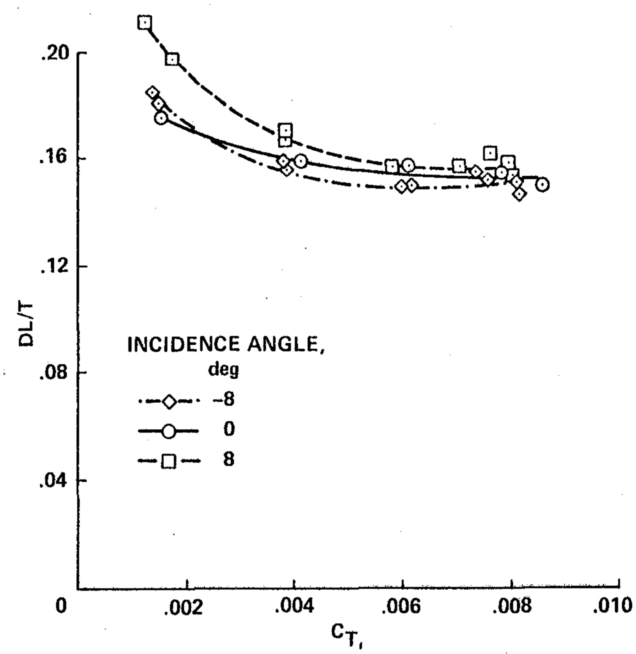

Figure 14. Effect of Wing Incidence Angle on Small-Scale Wing Download - δ_F = 0°.

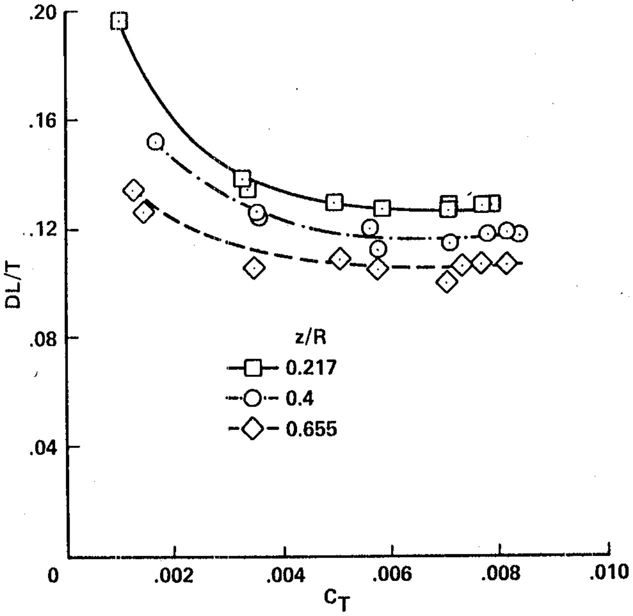

Figure 15. Effect of Distance Between Rotor and Wing on Wing Download.

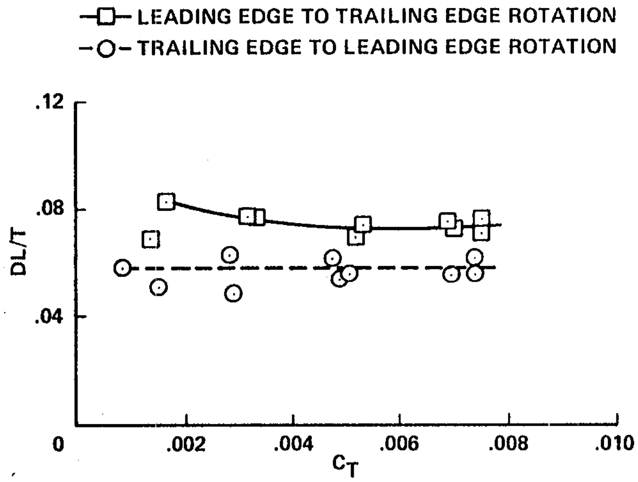

Figure 17. Effect of Rotor Rotation Direction on Wing Download.

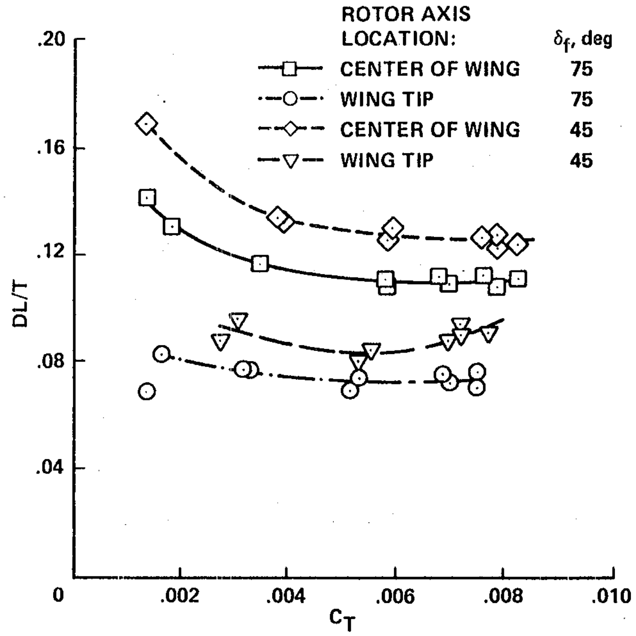

Figure 16. Effect of Rotor Position on Wing Download.

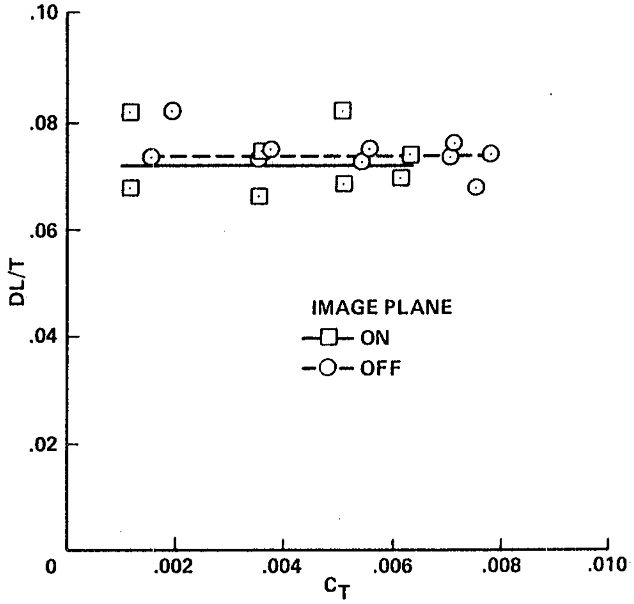

Figure 18. Effect of Image Plane on Download - z/R = 0.4.

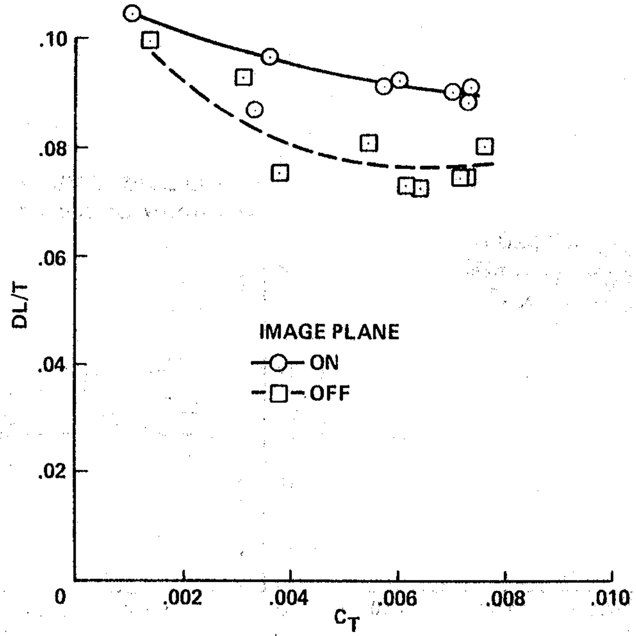

Figure 19. Effect of Image Plane on Download - z/R = 0.217.

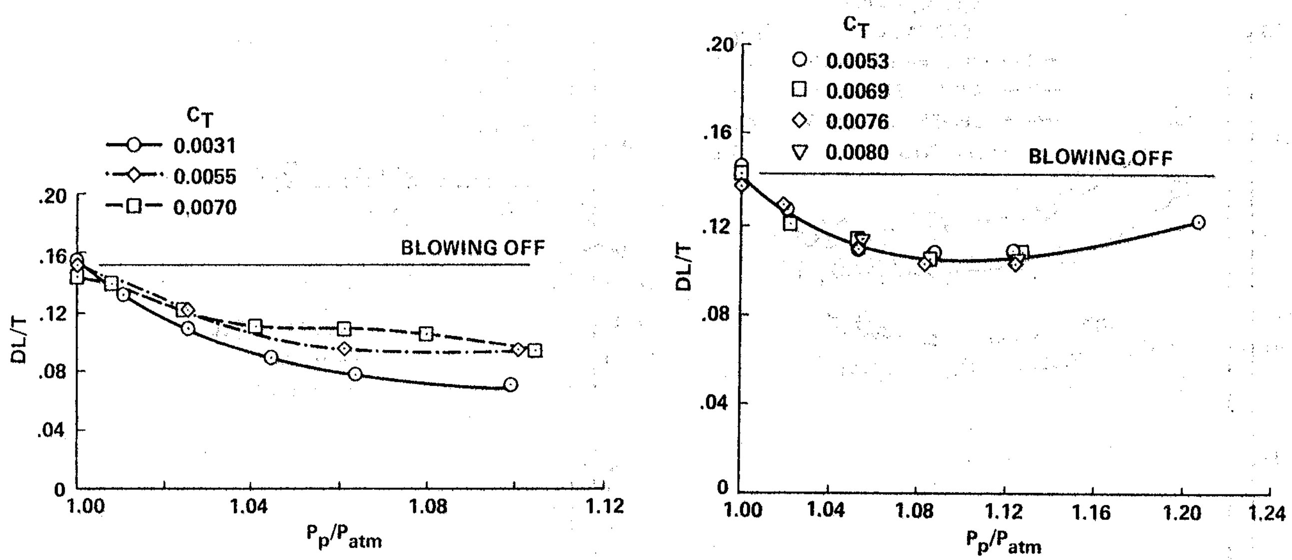

(a) h/c = 0.0014.

(b) h/c = 0.0010.

Figure 20. Effect of Blowing Pressure ratio on Download.

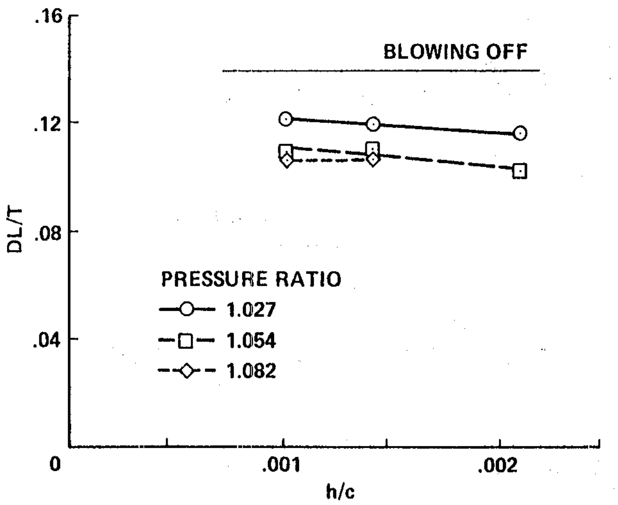

Figure 21. Effect of Blowing Slot Height on Download.

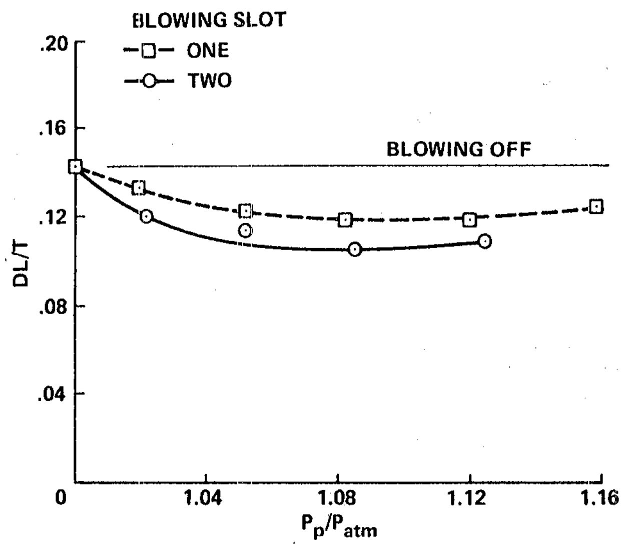

Figure 22. Comparison of Download with One and Two Blowing Slots.

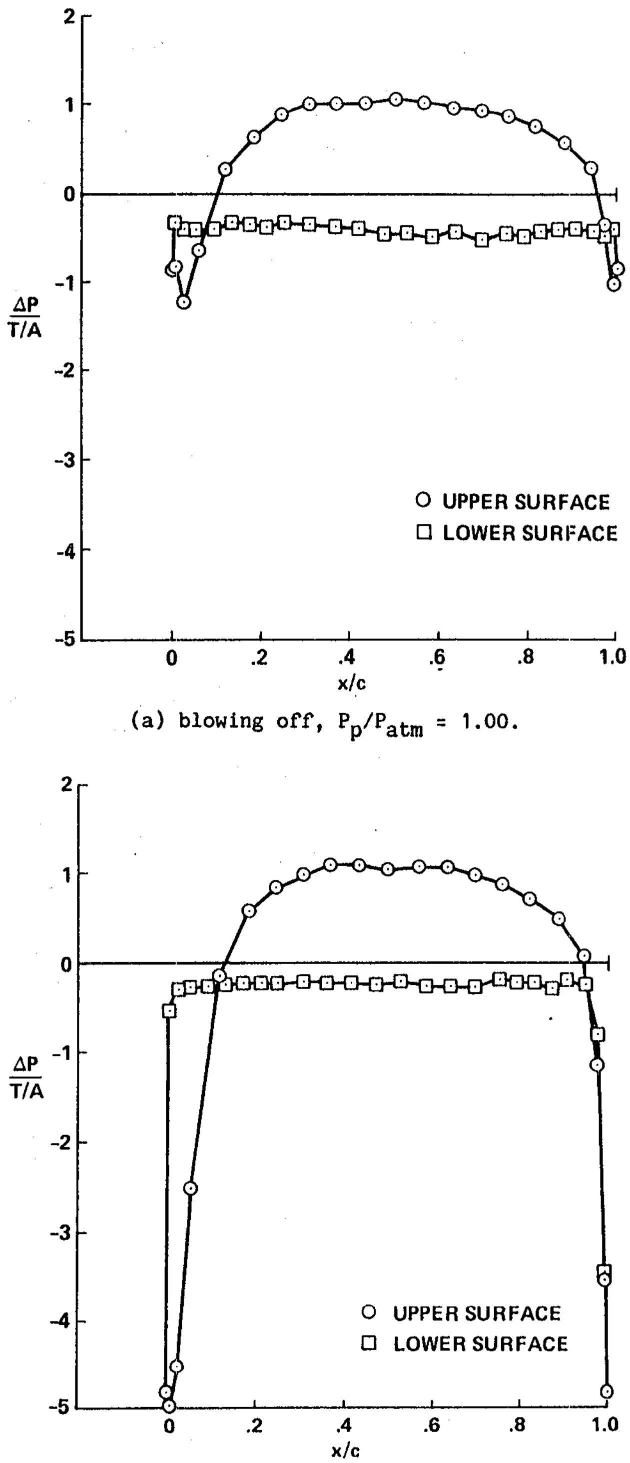

(a) blowing off, P_p/P_{atm} = 1.00.

(b) blowing on, P_p/P_{atm} = 1.09.

Figure 23. Circulation Control Wing Surface Pressures.

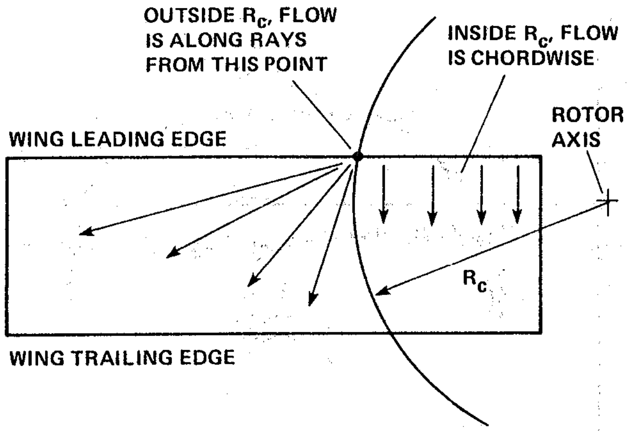

Figure 24. Wing Surface Flow Directions Used in Analysis.

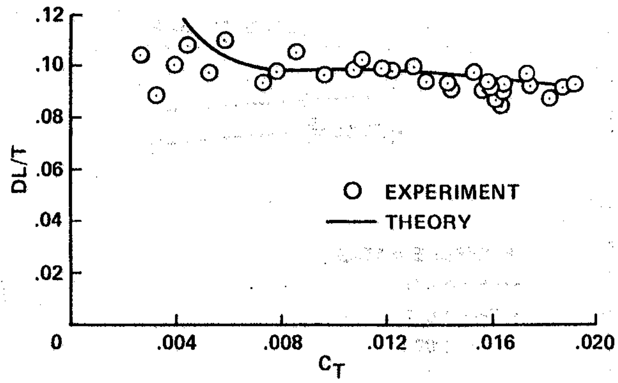

Figure 25. Comparison of Predicted V-22 Download with Large-Scale Test Data.

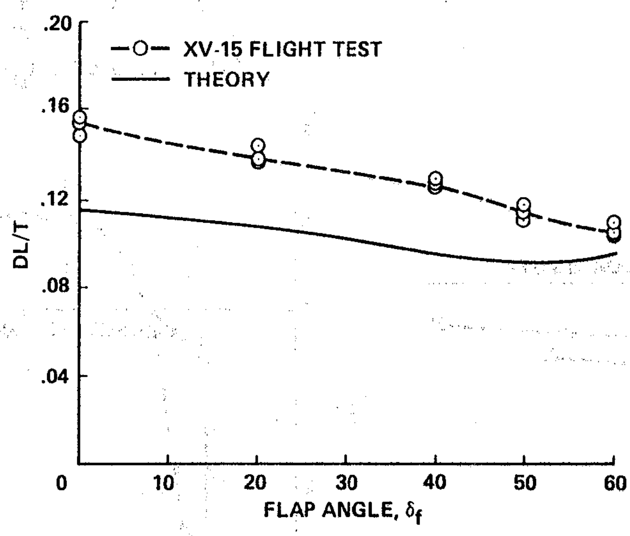

Figure 26. Comparison of Predicted Download with XV-15 Flight Test Data.

1. Report No.	2. Government Accession No.	3. Recipient's Catalog No.
NASA TM-88255		

4. Title and Subtitle	5. Report Date
ROTOR/WING AERODYNAMIC INTERACTIONS IN HOVER	May 1986
	6. Performing Organization Code
7. Author(s)	8. Performing Organization Report No.
Fort E. Felker and Jeffrey S. Light	A-86246
	10. Work Unit No.
9. Performing Organization Name and Address	11. Contract or Grant No.
Ames Research Center, Moffett Field, CA 94035	
	13. Type of Report and Period Covered
12. Sponsoring Agency Name and Address	Technical Memorandum
National Aeronautics and Space Administration, Washington, DC 20546	14. Sponsoring Agency Code: 505-61-51

15. Supplementary Notes

Point of contact: Fort E. Felker, Ames Research Center, M/S 247-1, Moffett Field, CA 94035 (415) 694-6096 or FTS 464-6096

16. Abstract

An experimental and theoretical investigation of rotor/wing aerodynamic interactions in hover is described. The experimental investigation consisted of both a large-scale and a small-scale test. A 0.658-scale, V-22 rotor and wing was used in the large-scale test. Wing download, wing surface pressure, rotor performance, and rotor downwash data from the large-scale test are presented. A small-scale experiment was conducted to determine how changes in the rotor/wing geometry affected the aerodynamic interactions. These geometry variations included the distance between the rotor and wing, wing incidence angle, and configurations both with the rotor axis at the tip of the wing (tilt rotor configuration) and with the rotor axis at the center of the wing (compound helicopter configuration). A wing with boundary-layer control was also tested to evaluate the effect of leading and trailing edge upper surface blowing on the wing download. A computationally efficient, semi-empirical theory was developed to predict the download on the wing. Finally, correlations between the theoretical predictions and test data are presented.

17. Key Words (Suggested by Author(s))	18. Distribution Statement
Tilt rotor Rotor performance Aerodynamic interactions Hover download	Unlimited Subject Category - 02

19. Security Classif. (of this report)	20. Security Classif. (of this page)	21. No. of Pages	22. Price*
Unclassified	Unclassified	27	A03

*For sale by the National Technical Information Service, Springfield, Virginia 22161

End of Document